Journal of Materials Chemistry A

Accepted Manuscript

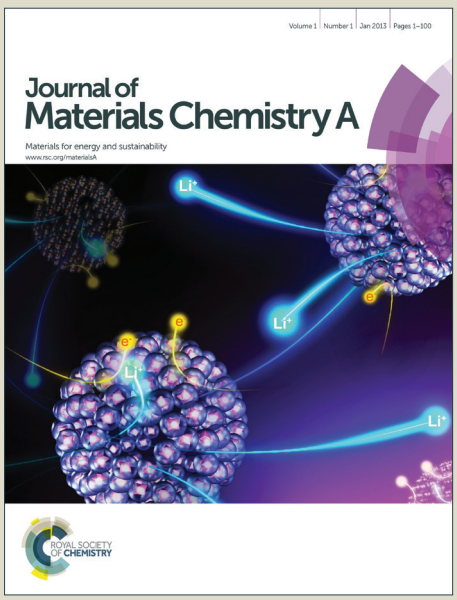

This is an *Accepted Manuscript*, which has been through the Royal Society of Chemistry peer review process and has been accepted for publication.

Accepted Manuscripts are published online shortly after acceptance, before technical editing, formatting and proof reading. Using this free service, authors can make their results available to the community, in citable form, before we publish the edited article. We will replace this *Accepted Manuscript* with the edited and formatted *Advance Article* as soon as it is available.

You can find more information about *Accepted Manuscripts* in the Information for Authors.

Please note that technical editing may introduce minor changes to the text and/or graphics, which may alter content. The journal's standard Terms & Conditions and the Ethical guidelines still apply. In no event shall the Royal Society of Chemistry be held responsible for any errors or omissions in this *Accepted Manuscript* or any consequences arising from the use of any information it contains.

ROYAL SOCIETY OF CHEMISTRY

www.rsc.org/materialsA

Scalable fabrication of exceptional 3D carbon networks for supercapacitors

Kuo Song,[†] Wei-Li Song,[†] Li-Zhen Fan,[†,*]

[†]*Institute of Advanced Materials and Technology, University of Science and Technology Beijing, Beijing, 100083, P. R. China.*

* Corresponding Authors: Tel/Fax: +86 10 6233-4311

Email: fanlizhen@ustb.edu.cn (Li-Zhen Fan)

Journal of Materials Chemistry A Accepted Manuscript

Abstract

Supercapacitors prepared by three-dimensional porous carbon networks, such as graphene- and carbon nanotube-based aerogels, have attracted extensive attention in wide fields. However, undesirable concerns, including high cost, complicated process, and insufficient yield, have greatly restricted their large-scale practical applications. In this study, a facile and exclusive approach is presented toward scalable preparation novel 3D porous carbon networks using relatively low-cost commercial cotton. Capacitive electrode materials for supercapacitors and corresponding flexible devices have been achieved based on tailoring the chemical composition, surface area and pore size distribution via conventional carbonization and activation. Such exceptional 3D porous carbon networks of controllable properties have shown high specific surface area up to 1563 m^2 g^{-1} and optimized energy storage capability of 314 and 170 F g^{-1} at current densities of 0.1 and 10 A g^{-1} in 6 mol L^{-1} KOH electrolyte, respectively. Consequently, these advantageous features allow them to be directly utilized in the flexible all-solid-state supercapacitors, which exhibites considerably sufficient energy storage performance and excellent cycling stability.

Key words: Porous carbon; 3D networks; supercapacitors; energy storage.

Journal of Materials Chemistry A Accepted Manuscript

1. Introduction

The serious pollution arisen from the nonrenewable fossil fuels, along with the increasing cost, have stimulated great research efforts for the storage and conversion of renewable energy sources. The fast-growing market for portable electronic devices and hybrid electronic vehicles has also demanded innovative energy storage materials of high power density and efficient energy conversion.[1-6] Electrochemical capacitors, also known as supercapacitors, are considered as promising candidate for energy storage device owing to the high power density, long cycle life, and fast charge/discharge processes,[2,7] and they are recently required to be lightweight, flexible, and effective for meeting the urgent requirement in the industry.[8-10] With various nanostructures or unique morphologies, a variety of carbon sources have been widely studied, aiming to improve the electrochemical capacitance and power density. Especially, 3D carbon porous networks have been recently pursued since they are considered to be the most promising electrode materials owing to their advantageous features of enhanced ionic and electronic transport, high specific capacities and superior long-term stability.[11-14]

Numerous synthesis techniques have been widely explored for preparing 3D carbon porous networks,[15-18] and they could be approximately divided into three categories: template methods,[18-20] chemical methods[21-25] and physical methods[26-30]. For the template methods, carbon nanotube (CNT)-carbon nanocup 3D hybrid structures have been proposed and synthetized by chemical vapor deposition using short channel anodized aluminum oxide templates. The assembled two-electrode supercapacitors based on the resultant materials showed an area specific capacity of 1 mF cm^{-2} in 1 mol L^{-1} $LiPF_6$ at a current of 10 μA.[19] As a typical example in the chemical methods, CNT- and graphene-based aerogels (GAs) with high electrical conductivity, large surface area and porous structures have been largely studied.[21-25, 31-32] Our group have prepared flexible solid-state supercapacitors based on 3D GA/porous carbon hybrid aerogels in the previous work, which presented increased specific capacity of 187 F g^{-1} at the current density of 1 A g^{-1} in the two-electrode polyvinylalcohol (PVA)/KOH gel electrolyte.[32] In the physical methods, active agents,

Journal of Materials Chemistry A Accepted Manuscript

such as KOH,[26-28, 33] $ZnCl_2$,[29] and H_3PO_4,[30] are generally employed to signficantly improve the porosities in the 3D carbon materials. For instance, a flexible porous carbon thin films have been prepared by KOH activation of reduced graphene oxide paper, and the as-fabricated two-electrode cell based the activated films delivered specific capacitance of 120 F g^{-1} at the current density of 10 A g^{-1} in the organic solution system.[33]

Although 3D porous carbon networks based on template-assistance and chemical synthesis have made substantial progress up to date, the remaining issues still limit their applications in the industry. On the one hand, the main challenges in the template synthesis should be the dependence of inorganic template materials, such as silica and zeolite, and associated complicated procedures for removing templates, which would essentially increase the cost in the practical application.[34-35] On the other hand, exploration of facile procedures for scalable preparing porous 3D CNTs- and graphene-based materials remains a great challenge.[8, 36-38] As a consequence, combination of a relatively low-cost raw material and a simply scalable approach seems to be the potential alternative for addressing the bottleneck.

In the present work, we demonstrate a simple and scalable method for preparing 3D carbon networks of high-performance supercapacitor electrode using relatively low-cost commercial cotton (Table S1 lists the price comparison) and easily controllable method. The as-prepared cotton-derived carbon networks (CCNs) have delivered favorable charge-discharge properties with high specific capacitance of 240 F g^{-1} in 6 mol L^{-1} KOH aqueous solution at the current density of 0.1 A g^{-1}, since the 3D networks has been well preserved in the entire treatments. Further improvements have been achieved by tailoring the porosity and chemical composition via KOH activation, with the purpose of engineering the interfaces, nanostructures, and electrochemical performance of the CCNs. The as-fabricated activated cotton-derived carbon networks (A-CCNs) were found to possess much enlarged specific surface area with increased micropores and channels for ionic diffusion and electronic transfer. Thus, they were able to present an increased specific capacitance (314, 215, and 170 F g^{-1} at current densities of 0.1, 1, and 10 A g^{-1}, respectively) and excellent cycling stability

Journal of Materials Chemistry A Accepted Manuscript

(retention up to 96% after 10,000 cycles). The results of flexible all-solid state device indicate that the facile procedures hold great potential in the energy storage industry.

2. Experimental sections

2.1 Synthesis of CCNs and A-CCNs

The commercial cotton was directly used as the starting material without any further pre-treatment. Typically, a piece of cotton was cut into a certain shape (determined by the furnace size) and subjected to carbonization at 900 ^{o}C for 2 h with a heating rate of 5 ^{o}C min^{-1} under N_2 atmosphere. The resulting samples (CCNs) were further treated under ultrasonication for 1 h with the presence of mixture of HNO_3/H_2SO_4 (v/v=1/3) in order to improve the hydrophilicity. The resulted samples were then immersed in the aqueous solution of KOH, and then dried at 90 ^{o}C overnight to make water evaporation, thoroughly. The mixtures were then thermally annealed at 800 ^{o}C for 1 h in N_2 with a heating rate of 5 ^{o}C min^{-1}. The resulted samples (A-CCNs) were washed with 10 wt% HCl aqueous solution and deionized water, and then dried at 90 ^{o}C. The predetermined mass ratio of CCNs and KOH were 1:1, 1:2, 1:4, respectively (abbreviated as A-CCNs-1:1, A-CCNs-1:2, and A-CCNs-1:4).

2.2 Fabrication of three-electrode system and two-electrode devices

The electrochemical performance of the carbon materials was determined in a three-electrode cell with basic aqueous solutions. The working electrode was prepared by mixing the carbon samples, acetylene black with poly (tetrafluoroethylene) in a weight ratio of 80:15:5, and then the mixture was pressed onto nickel foam. The typical mass and dimensions of the working electrodes are 10 mg and 1 cm^2. For the three-electrode system, Pt and Hg/HgO electrode were used as the counter electrode and reference electrode, respectively, while the KOH solution (6 mol L^{-1}) was employed as the electrolyte.

The electrochemical performance of A-CCNs was further determined in a gel electrolyte by using a two-electrode cell. In a typical preparation, PVA powder (2 g) was dissolved in distilled water (20 mL) under vigorous stirring at 85 ^{o}C. Until a stable PVA aqueous solution was formed, two working electrodes with PVA aqueous solution in between were stacked, followed by adding excessive KOH

Journal of Materials Chemistry A Accepted Manuscript

aqueous solution (6 mol L^{-1}). The PVA-based gel, which acted as the electrolyte and separator, was settled for 24 h, allowing them to form a robust flexible all-solid-state device.

2.3 Characterization

The morphologies of synthesized composite materials were observed by a field emission scanning electron microscopy (FE-SEM, JEOL JSM-6330). Transmission electron microscopy (TEM) images were obtained by JEM-2100F TEM system. N_2 adsorption-desorption isotherms were carried out using Quantachrome Autosorb-IQ2 analyzer at 77 K after being degassed at 300 ^{o}C for at least 3 h. X-ray photoelectron spectroscopy (XPS) was acquired on PHI-5300.

Galvanostatic charge/discharge was tested at various current densities using LAND-CT2001A (Wuhan Jinnuo Electronics. Ltd.). Cyclic voltammetry (CV) was carried out using a CHI660C electrochemical workstation (Shanghai Chenhua).

3. Results and discussion

In the typical preparation of 3D carbon networks (Figure 1), a piece of commercial cotton was used as the raw material without any pretreatment (Figure 1a), and the corresponding amount and size could be easily extended for scalable production according to the requirement. For preparing CCNs (Figure 1b), the cotton was directly heated up for carbonization under nitrogen atmosphere, and then further treated in the mixed acid solution under sonication to improve the hydrophilicity. The A-CCNs of 3D porous networks were obtained by calcining the mixture of CCNs and KOH (Figure 1c).

In the design of such novel 3D carbon networks, utilization of the commercial cotton as the raw materials for achieving A-CCNs shows several exclusive favorable characteristics. Firstly, because of simply, good controllability and environmental-friendly, the entire process could be easily scaled up for meeting the industrial demands. Secondly, analogous to typical 3D nanostructures based on CNT and graphene, porous CCNs (including A-CCNs) could facilitate the electron transfer and provide convenient channels for ionic diffusion in the interspaces. Thirdly, the introduced hierarchical porosities (including micro-, meso-, and macropores) are expected to essentially provide more

Journal of Materials Chemistry A Accepted Manuscript

contact sites for electrolyte ions, substantially promoting the ionic exchange rate in the electrode/electrolyte interfaces.

Figure 2 exhibits typical SEM and TEM images of the CCNs (Figure 2a and 2e) and A-CCNs (Figure 2b-2d, and 2f). As presented in Figure 2a, the CCNs presented typical 3D networks structure. Compared to the CCNs (the inset in Figure 2a), pronounced wrinkles were expected to be observed on the rough surface of the A-CCNs (Figure 2b-d). Such morphological changes should be associated with different degrees of KOH etching, and meanwhile the surface etching degree increases with the KOH concentration. Representative TEM images of CCNs (Figure 2e) and A-CCNs-1:2 (Figure 2f) indicate that the diffraction contrast implies the presence of the nano-scale pores and wrinkles in A-CCNs-1:2, enabling it to present large specific surface area and favorable pathways for ionic diffusion.

The nitrogen adsorption/desorption isotherms of the cotton-derived carbon materials are presented in Figure 3a. Compared to the CCNs, A-CCNs have a much higher N_2 sorption capacity, which displayed type I sorption isotherms characteristic for microporous materials.[6] In the low pressure region (P/P_0=0~0.1), it is clear to observe the rapid increase of the adsorption in the A-CCNs, consistent with the observation in the CCNs, which indicates a large amount of micropores.[33,39]. The surface area of micropores (S_{mirco}) in the A-CCNs-1:2 indicates a significant increase in comparison with the CCNs (Table 1). The direct comparison shows that the A-CCNs-1:2 possess smaller specific surface area than the A-CCNs-1:1 and A-CCNs-1:4, which is linked to the changes of the carbon nanostructures and configurations in the KOH activation, carbonization and acid treatments.[14, 40] In addition, A-CCNs-1:4 presented smaller surface area than A-CCNs-1:1, which maybe attributed to the structural collapse caused by over-etching. Moreover, pore size distribution (Figure 3b) and micropore volume (Table 1) were calculated by the density functional theory (DFT) method.[6] The estimated average pore size of A-CCNs-1:2 was calculated to be 1.791 nm (Table 1), which is the major feature of micropores (<2 nm). Consequently, the results here suggest that A-CCNs has substantially enhanced the surface area by KOH activation and increased the amount of micropores

Journal of Materials Chemistry A Accepted Manuscript

(typically in A-CCNs-1:2).

XPS was carried out to investigate the surface chemical compositions of the samples. Figure 4 (a-d) exhibit the C 1s spectra of CCNs, A-CCNs-1:1, A-CCNs-1:2, and A-CCNs-1:4, respectively, demonstrating pronounced carbon-carbon species (~284.6 eV) in both samples.[41] Compared to CCNs, slightly enhanced C-O (~286.1 eV) and C-N (~286.33 eV) peaks have been found in A-CCNs due to the process of activation, which refers to oxygen containing functional groups (such as hydroxyl and carboxyl groups), mainly making contributions to increasing specific storage by means of pseudocapacitive interaction. [6, 39] In addition, it is noticeable that the substantial increase of nitrogen content in A-CCNs shown in Figure 4, which could lead to further enhancement in the specific capacity [42-44]. Further XRD patterns of CCNs, A-CCNs-1:1, A-CCNs-1:2, and A-CCNs-1:4 were described in Figure S1. XRD patterns of the A-CCNs are similar to those of CCNs, showing a broad peak at about 26°, consistent with amorphous carbon structure. Because of such typical 3D porous carbon nanostructures, they are expected to act as ideal electrode materials for supercapacitors in the 6 mol L^{-1} KOH aqueous solution. Figure 5a shows the typical CV curves of CCNs and A-CCNs at 10 mV s^{-1}. The curves demonstrate quasi-rectangular shape with slight distortion, which is induced by the pseudo-capacitance owing to the oxygen- and nitrogen-containing functional groups. In comparison with the CCNs, A-CCNs apparently have a much larger area (Figure 5a), indicating increased electrochemical performance and enhanced energy storage capability. According to Figure 5b, the galvanostatic charge-discharge curves illustrate almost isosceles triangles at the current density of 1 A g^{-1}, which suggests typical double-layer capacitance with no distinct voltage drop. The specific capacitance could be calculated according to the equation of $C_s = I \times t/V/m$,[2] where C_s (F g^{-1}) is the specific capacity, I (A g^{-1}) the response current density, t (s) the discharge time, V (V) the potential and m (g) the mass of active materials. Therefore, the results in Figure 5b suggest that the A-CCNs deliver substantially enhanced energy storage capability compared to CCNs. Moreover, the relationship of the specific capacitance with respect to the charge/discharge specific currents (Figure 5c) manifest that the A-CCNs-1:2 possess much enhanced

Journal of Materials Chemistry A Accepted Manuscript

capacities up to 314, 215 and 170 F g^{-1} at current densities of 0.1, 1 and 10 A g^{-1}, respectively, compared to the values found in the CCNs (240, 158 and 92 F g^{-1} at 0.1, 1 and 10 A g^{-1}, respectively). Consequently, such considerable enhancement in the energy storage should be associated with chemical compositions and nanostructures of the 3D porous carbon networks. Moreover, such electrode shows a high retention up to 98% after 10,000 cycles at a current density of 3 A g^{-1}（95% after 10,000 cycles at 10 A g^{-1}）, indicating excellent long-term cycling stability (Figure 5d).

The A-CCNs-1:2 were further processed into a symmetrical two-electrode system to fabricate a flexible all-solid-state supercapacitor.[14,32] A diagram of the supercapacitor using A-CCNs-1:2 as electrodes with a polymer electrolyte gel as the electrolyte and separator was shown in Figure 6a. The specific capacitance of the two-electrode device was calculated by the equation of $C_s = 2I \times t/V/m$,[31] where m is the mass of the A-CCNs-1:2 in one electrode. Figure 6b exhibits the CV curves at 5 mV s^{-1} of the flexible device under different bending angles and no significant change was observed, indicating excellent capacitance retention upon compression. As shown in Figure 6c, the CV curves exhibit no pronounced redox peaks at different current densities, presenting typical double-layer capacitive behavior. According to the galvanostatic charge/discharge curves in Figure 6d, similar isosceles triangles at different current densities were also observed, without distinct voltage drop presented. Figure 6e displays the rate stability of the all-solid-state supercapacitor, showing the highest capacitance up to 120 F g^{-1} at the current density of 3 A g^{-1}. Additionally, the all-solid-state supercapacitor also presented excellent cycling stability with 96% retention after 10,000 cycles at a current density of 3 A g^{-1} (92% after 10,000 at 10 A g^{-1}) (Figure 6f).

As aforementioned, the as-prepared 3D carbon networks show very similar morphologies to CNT- or graphene-based 3D nanostructures[45-53]. Based on the sufficient surface area of the 3D carbon networks, this work has proposed a different view on the achievement of the porous carbon structures and subsequent improvements in the electrochemical performance. Compared to the performance in the three-electrode systems (Table 2), the optimized electrochemical performance of the A-CCNs-1:2 competes well and is even higher than that of some typical CNT- or graphene-based

Journal of Materials Chemistry A Accepted Manuscript

3D nanostructures[45-53]. It is suggested that A-CCNs based on the facile activation process are able to afford as sufficient surface area as the commercial CNT- and graphene-based 3D nanostructures, with considerably effective electrically conductive networks for promoting electronic transport. Moreover, the price advantages listed in Table S1 further suggest that such relatively low-cost 3D porous carbon networks that enable to offer sufficient specific capacitance similar to the commercially available carbon materials are more advantageous in the extension for scalable fabrication. According to the results in the current work, there is still room for performance improvements, including adjusting carbonization parameters and tailoring the activation conditions, and thus much enhanced carbon-based energy-storage devices could be envisaged.

4. Conclusion

In conclusion, we have demonstrated a facile and low-cost approach toward engineering the commercially available cotton into 3D porous carbon networks via conventional carbonization and activation. Similar to the widely used CNT- and graphene-based capacitor electrodes, the as-prepared A-CCNs were found to present advantageous features in the nanostructures, chemical compositions, pore diameter distribution, and specific surface areas. Therefore, the A-CCNs could deliver excellent electrochemical performance and energy storage capability. Comparison of other CNT- and graphene-based 3D nanostructures indicates that the A-CCNs based on a more simple strategy coupled with competitive electrochemical performance have promised great potential in the scalable fabrication of high-performance 3D porous carbon materials that are potentially extended in energy storage industry.

Acknowledgements

Financial support from 973 Project (2013CB934001 and 2015CB932500), NSF of China (51172024, 51372022, and 51302011), Ministry of Education (20130006110019) and the Fundamental Research Funds for the Central Universities (FRF-TP-09-007A and FRF-TP-14-091A2) are gratefully acknowledged.

Journal of Materials Chemistry A Accepted Manuscript

References

1. J. R. Miller, P. Simon, *Science*, 2008, **321**, 651-652.
2. P. Simon, Y. Gogotsi, *Nat. Mater.*, 2008, **7**, 845-854.
3. G. P. Wang, L. Zhang, J. J. Zhang, *Chem. Soc. Rev.*, 2012, **41**, 792-828.
4. P. Simon, Y. Gogotsi, *Accounts Chem. Res.*, 2013, **46**, 1094-1103.
5. Y. P. Zhai, Y. Q. Dou, D. Y. Zhao, P. F. Fulvio, R. T. Mayes, S. Dai, *Adv. Mater.*, 2011, **23**, 4828-4850.
6. L. Zhao, L. Z. Fan, M. Q. Zhou, H. Guan, S. Y. Qiao, M. Antonietti, M. M. Titirici, *Adv. Mater.*, 2010, **22**, 5202-5206.
7. Y. Gogotsi, P. Simon, *Science*, 2011, **334**, 917-918.
8. M. F. El-Kady, V. Strong, S. Dubin, R. B. Kaner, *Science*, 2012, **335**, 1326-1330.
9. Y. Xu, X. Lin, Z. Y. Zhong, X. Huang, X. Q. Weiss, O. Nathan, X. F. Duan, *Nat. Commun.*, 2014, **5**, 4554-4561.
10. Z. S. Wu, K. Parvez, X. L. Feng, K. Mullen, *Nat. Commun.*, 2013, **4**, 2487-2494.
11. H. Jiang, P. S. Lee, C. Li, *Energy Environ. Sci.*, 2013, **6**, 41-53.
12. S. Chabi, C. Peng, D. Hu, Y. Zhu, *Adv. Mater.*, 2014, **26**, 2440-2445.
13. S. H. Aboutalebi, R. Jalili, D. Esrafilzadeh, M. Salari, Z. Gholamvand, S. A. Yamini, K. Konstantinov, R. L. Shepherd, J. Chen, S. E. Moulton, *ACS Nano*, 2014, **8**, 2456-2466.
14. W. L. Song, K. Song, L. Z. Fan, *ACS Appl. Mater. Interfaces,* 2015, **7**, 4257-4264.
15. T. Kyotani, T. Nagai, S. Inoue, A. Tomita, *Chem. Mater.*, 1997, **9**, 609-615.
16. A. Ahmadpour, D. D. Do, *Carbon*, 1996, **34**, 471-479.
17. X. C. Gui, J. Q. Wei, K. L. Wang, A. Y. Cao, H. W. Zhu, Y. Jia, Q. K. Shu, D. H. Wu, *Adv. Mater.*, 2010, **22**, 617-621.
18. H. Nishihara, T. Kyotani, *Adv. Mater.*, 2012, **24**, 4473-4498.
19. M. G. Hahm, A. L. M. Reddy, D. P. Cole, M. Rivera, J. A. Vento, J. Nam, H. Y. Jung, Y. L. Kim, N. T. Narayanan, D. P. Hashim, C. Galande, Y. J. Jung, M. Bundy, S. Karna, P. M. Ajayan

Journal of Materials Chemistry A Accepted Manuscript

and R. Vajtai, *Nano Lett.*, 2012, **12**, 5616-5621.

20. C. Yu, J. Fan, B. Tian, D. Zhao, G. D. Stucky, *Adv. Mater.*, 2002, **14**, 1742-1745.

21. X. L. Wu, A. W. Xu, *J. Mater. Chem. A*, 2014, **2**, 4852-4864.

22. J. Hu, Z. Kang, F. Li, X. Huang, *Carbon*, 2014, **67**, 221-229.

23. X. H. Cao, Z. Y. Yin, H. Zhang, *Energy Environ. Sci.*, 2014, **7**, 1850-1865.

24. Z. Q. Niu, W. Y. Zhou, J. Chen, G. X. Feng, H. Li, W. J. Ma, J. Z. Li, H. B. Dong, Y. Ren, D. Zhao, S. S. Xie, *Energy Environ. Sci.*, 2011, **4**, 1440-1446.

25. T. Chen, L. M. Dai, *J. Mater. Chem. A*, 2014, **2**, 10756-10775.

26. Y. W. Zhu, S. Murali, M. D. Stoller, K. J. Ganesh, W. W. Cai, P. J. Ferreira, A. Pirkle, R. M. Wallace, K. A. Cychosz, M. Thommes, D. Su, E. A. Stach, R. S. Ruoff, *Science*, 2011, **332**, 1537-1541.

27. J. C. Wang, S. Kaskel, *J. Mater. Chem.*, 2012, **22**, 23710-23725.

28. A. Bello, F. Barzegar, D. Momodu, J. Dangbegnon, F. Taghizadeh, N. Manyala, *Electrochim. Acta*, 2015, **151**, 386-392.

29. T. Wang, S. Tan, C. Liang, *Carbon*, 2009, **47**, 1880-1883.

30. Q. S. Liu, T. Zheng, P. Wang, L. Guo, *Ind. Crops. Prod.*, 2010, **31**, 233-238.

31. Y. X. Xu, Z. Y. Lin, X. Q. Huang, Y. Liu, Y. Huang, X. F. Duan, *ACS Nano*, 2013, **7**, 4042-4049.

32. H. F. Ju, W. L. Song, L. Z. Fan, *J. Mater. Chem. A*, 2014, **2**, 10895-10903.

33. L. L. Zhang, X. Zhao, M. D. Stoller, Y. W. Zhu, H. X. Ji, S. Murali, Y. P. Wu, S. Perales, B. Clevenger, R. S. Ruoff, *Nano Lett.*, 2012, **12**, 1806-1812.

34. T. Kyotani, Z. Ma, A. Tomita, *Carbon*, 2003, **41**, 1451-1459.

35. B. Basavalingu, J. M. C. Moreno, K. Byrappa, Y. G. Gogotsi, M. Yoshimura, *Carbon*, 2001, **39**, 1763-1766.

36. Y. Ito, C. Christodoulou, M. V. Nardi, N. Koch, H. Sachdev, K. Müllen, *ACS Nano*, 2014, **8**, 3337-3346.

37. A. L. Higginbotham, D. V. Kosynkin, A. Sinitskii, Z. Sun, J. M. Tour, *ACS Nano*, 2010, **4**,

Journal of Materials Chemistry A Accepted Manuscript

2059-2069.

38. J. W. Zhu, C. Cheng, X. W. Yang, Y. F. Wang, L. Qiu, D. Li, *Chem-Eur. J.*, 2013, **19**, 3082-3089.

39. L. Z. Fan, S. Y. Qiao, W. L. Song, M. Wu, X. B. He, X. H. Qu, *Electrochim. Acta*, 2013, **105**, 299-304.

40. S. Stankovich, D. A. Dikin, R. D. Piner, K. A. Kohlhaas, A. Kleinhammes, Y. Jia, Y. Wu, S. T. Nguyen, R. S. Ruoff, *Carbon*, 2007, **45**, 1558-1565.

41. M. Kruk, M. Jaroniec, *Chem. Mater.*, 2001, **13**, 3169-3183.

42. D. Hulicova-Jurcakova, M. Seredych, G. Q. Lu, T. J. Bandosz, *Adv. Funct. Mater.*, 2009, **19**, 438-447.

43. Y. H. Lee, K. H. Chang, C. C. Hu, *J. Power Sources*, 2013, **227**, 300-308.

44. M. M. Zhang, R. Li, X. X. Chang, C. Xue, X. L. Gou, *J. Power Sources*, 2015, **290**, 25-34.

45. Y. M. Ren, J. M. Zhang, Q. Xu, Z. M. Chen, D. Y. Yang, B. Wang, Z. Jiang, *RSC Adv.*, 2014, **4**, 23412-23419.

46. J. H. Lee, N. Park, B. G. Kim, D. S. Jung, K. Im, J. Hur, J. W. Choi, *ACS Nano*, 2013, **7**, 9366-9374.

47. Z. B. Lei, F. H. Shi, L. Li, *ACS Appl. Mater. Interfaces*, 2012, **4**, 1058-1064.

48. W. L. Song, K. Song, L. Z. Fan, *ACS Appl. Mater. Interfaces*, 2015, **7**, 4257-4264.

49. C. Y. Yang, J. L. Shen, C. Y. Wang, H. J. Fei, H. Bao, G. C. Wang, *J. Mater. Chem. A*, 2014, **2**, 1458-1464.

50. G. Y. Zhu, Z. He, J. Chen, J. Zhao, X. M. Feng, Y. W. Ma, Q. L. Fan, L. H. Wang, W. Huang, *Nanoscale*, 2014, **6**, 1079-1085.

51. H. F. Ju, W. L. Song, L. Z. Fan, *J. Mater. Chem. A*, 2014, **2**, 10895-10903.

52. Z. S. Wu, Y. Sun, Y. Z. Tan, S. B. Yang, X. L. Feng, K. Müllen, *J. Am. Chem. Soc.*, 2012, **134**, 19532-19535.

53. Z. Y. Zhang, F. Xiao, Y. L. Guo, S. Wang, Y. Q. Liu, *ACS Appl. Mater. Interfaces*, 2013, **5**, 2227-2233.

Journal of Materials Chemistry A Accepted Manuscript

Table 1. Pore structure parameters of CCNs and A-CCNs-1:1, A-CCNs-1:2 and A-CCNs-1:4.

Sample	S_{total}	S_{micro} ($m^2 g^{-1}$)	$S_{meso+macro}$	V_{total}	V_{micro} ($cm^3 g^{-1}$)	$V_{meso+macro}$	APS [a] (nm)
CCNs	376.3	332	44.3	0.205	0.134	0.071	2.181
A-CCNs-1:1	1563	1452	111	0.876	0.695	0.181	2.242
A-CCNs-1:2	986.7	943.1	43.6	0.442	0.378	0.064	1.791
A-CCNs-1:4	1221	1124	97	0.664	0.528	0.136	2.176

Note: The surface areas for total (S_{total}) and micropores (S_{micro}) were obtained from multipoint Brumauer−Emmett−Teller (BET) plot and V−t plot, respectively, and the surface area of meso/macropore ($S_{meso+macro}$) was acquired by subtracting S_{micro} from S_{total}. Total pore volume (V_{total}) was determined at $P/P_0 = 0.99$, and micropore volume (V_{micro}) was calculated from V−t plot. The algorithm of meso/macropore ($V_{meso+macro}$) was similar with $S_{meso+macro}$; [a] Average Pore Size.

Journal of Materials Chemistry A Accepted Manuscript

Table 2. Electrochemical performance achieved in the typical CNT- and graphene-based 3D frameworks in three-electrode systems.

Electrode materials (Type)	Specific capacitance	Electrolytes	Cycling stability	Refs
A-CCNs-1:2	314 F g^{-1} (0.1 A g^{-1}) 215 F g^{-1} (1 A g^{-1}) 170 F g^{-1} (10 A g^{-1})	3M KCl	98% (10000)	This work
N-doped Carbonaceous aerogel	150.6 F g^{-1} (0.2 A g^{-1})	6 M KOH	-	42
cMR-rGO	210 F g^{-1} (0.1 A g^{-1}) 180 F g^{-1} (5 A g^{-1}) 160 F g^{-1} (10 A g^{-1})	1M $LiPF_6$ EC/DEC	96% (20000)	43
MnO_2/CNT/RGO	193 F g^{-1} (0.2 A g^{-1})	1 M Na_2SO_4	~70% (1300)	44
N-C-RGO-Networks	1320 F g^{-1} (0.1 A g^{-1}) 250 F g^{-1} (1 A g^{-1}) 200 F g^{-1} (10 A g^{-1})	6 M KOH	>92% (10000)	45
RGO/cMWCNT	193 F g^{-1} (1 A g^{-1}) 180 F g^{-1} (5 A g^{-1})	PAAK/KCl gel electrolyte	-	46
MnO2/CNT/grahene/Ni	251 F g^{-1} (1 A g^{-1})	1M Li_2SO_4	82% (3000)	47
GN/PC aerogels	324 F g^{-1} (0.1 A g^{-1}) 200 F g^{-1} (5 A g^{-1}) 190 F g^{-1} (10 A g^{-1})	6M KOH	＞90%（10000）	48
GA-MC	226 F g^{-1} (1 mV s^{-1}) 83 F g^{-1} (100 mV s^{-1})	1M H_2SO_4	140% (5000)	49
TiO_2/RGO hydrogel	206.7 F g^{-1} (0.5 A g^{-1}) 120 F g^{-1} (5 A g^{-1})	0.5 M Na_2SO_4	>99% (2000)	50

Journal of Materials Chemistry A Accepted Manuscript

Figure captions:

Figure 1. Schematic illustration of the fabrication procedures of the 3D porous networks and corresponding digital photographs: the raw material of commercial cotton (a), carbonized cotton after calcination (b), activated carbonized cotton via KOH activation (c).

Figure 2. Typical SEM micrographs of CCNs (a), A-CCNs-1:1 (b), A-CCNs-1:2 (c), and A-CCNs-1:4 (d), the inset is the high-magnification of selected area. TEM images of CCNs (e) and A-CCNs-1:2 (f).

Figure 3. N_2 adsorption-desorption isotherms (a) and DFT pore-size distribution (b) of the CCNs, A-CCNs-1:1, A-CCNs-1:2, and A-CCNs-1:4.

Figure 4. C 1s XPS spectra of the CCNs (a), A-CCNs-1:1 (b), A-CCNs-1:2 (c), and A-CCNs-1:4 (d), respectively.

Figure 5. Electrochemical properties of the CCNs and A-CCNs electrodes using a three-electrode cell in the 6 mol L^{-1} KOH aqueous solution: CV curves at a scan rate of 10 mV s^{-1} (a), typical galvanostatic charge-discharge curves at a current density of 1 A g^{-1} (b), relationship of the specific capacitance with respect to the charge/discharge specific currents (c), cycle stability of the A-CCNs-1:2 at current densities of 3 and 10 A g^{-1} (d).

Figure 6. Design and electrochemical performance of a flexible all-solid-state supercapacitor with A-CCNs-1:2 as electrodes. A diagram of the supercapacitor using A-CCNs-1:2 as electrodes with a polymer electrolyte gel as the electrolyte and separator (a), CV curves at 5 mV s^{-1} under different bending angles (b), CV curves at different scanning rates (c), typical galvanostatic charge-discharge curves at different current densities (d), specific capacitance of at different current densities (e), cycling stability of the flexible device at current densities of 3 and 10 A g^{-1} (f).

Journal of Materials Chemistry A Accepted Manuscript

Figures:

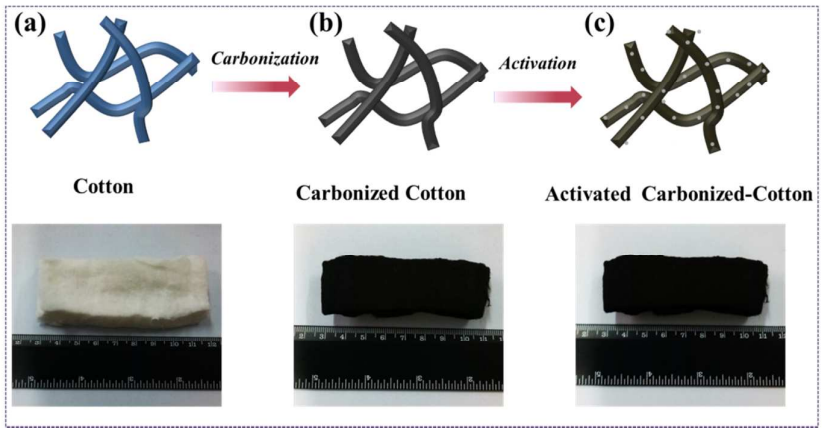

Figure 1

Journal of Materials Chemistry A Accepted Manuscript

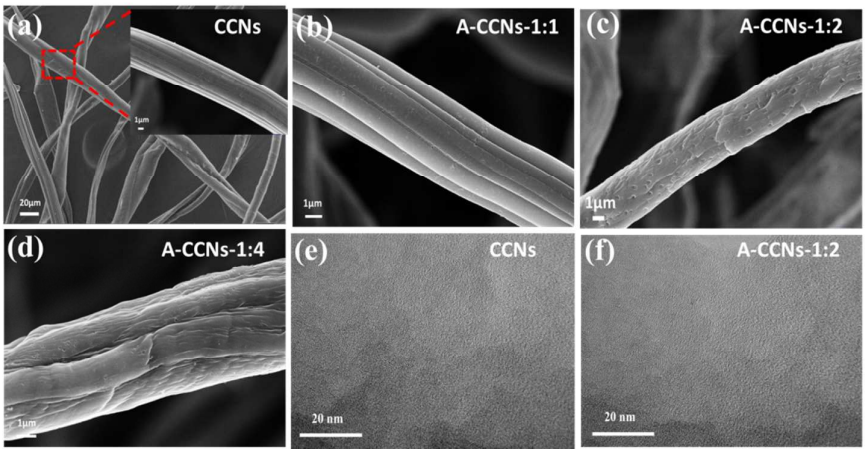

Figure 2

Journal of Materials Chemistry A Accepted Manuscript

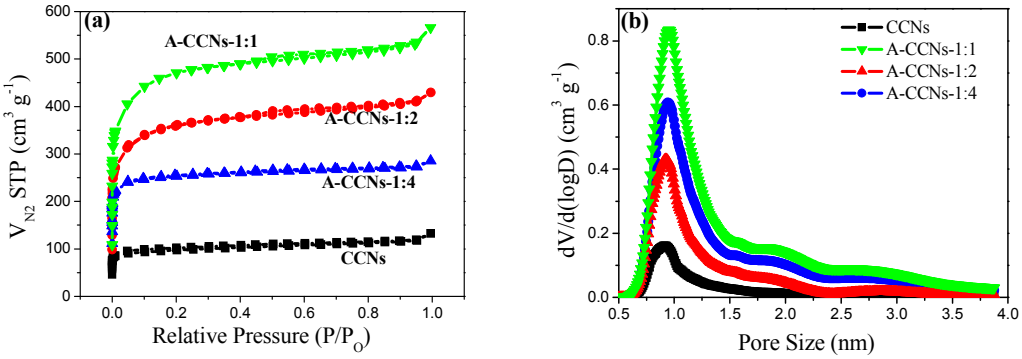

Figure 3

Journal of Materials Chemistry A Accepted Manuscript

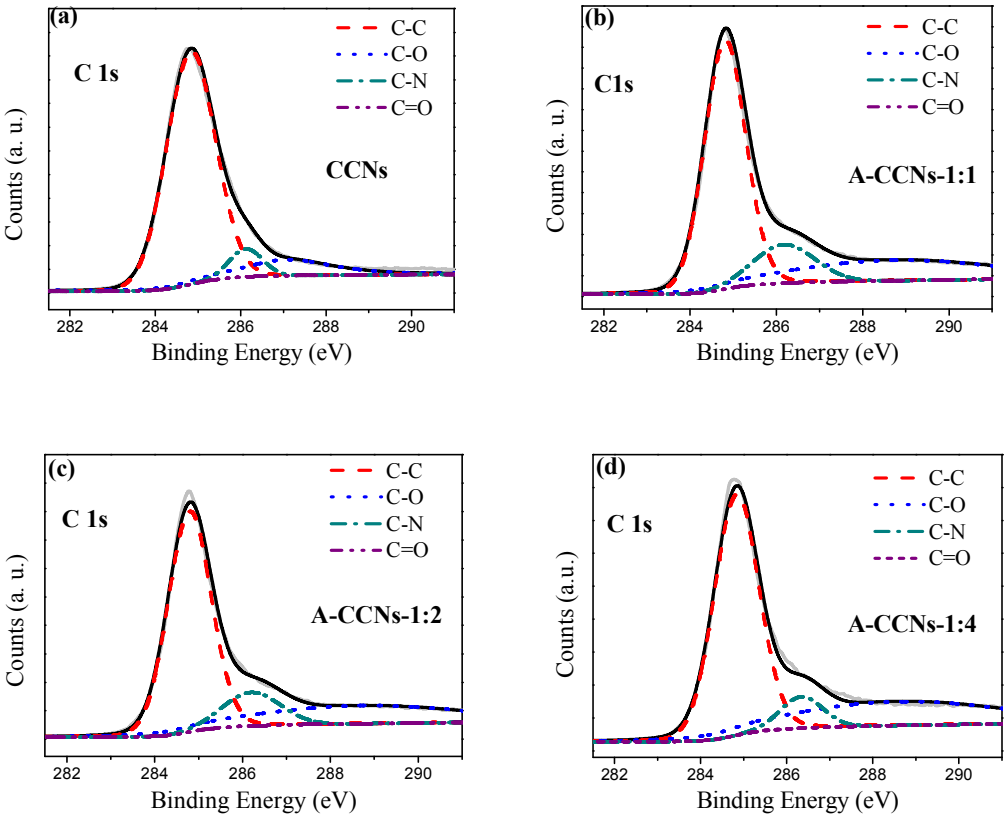

Figure 4

Journal of Materials Chemistry A Accepted Manuscript

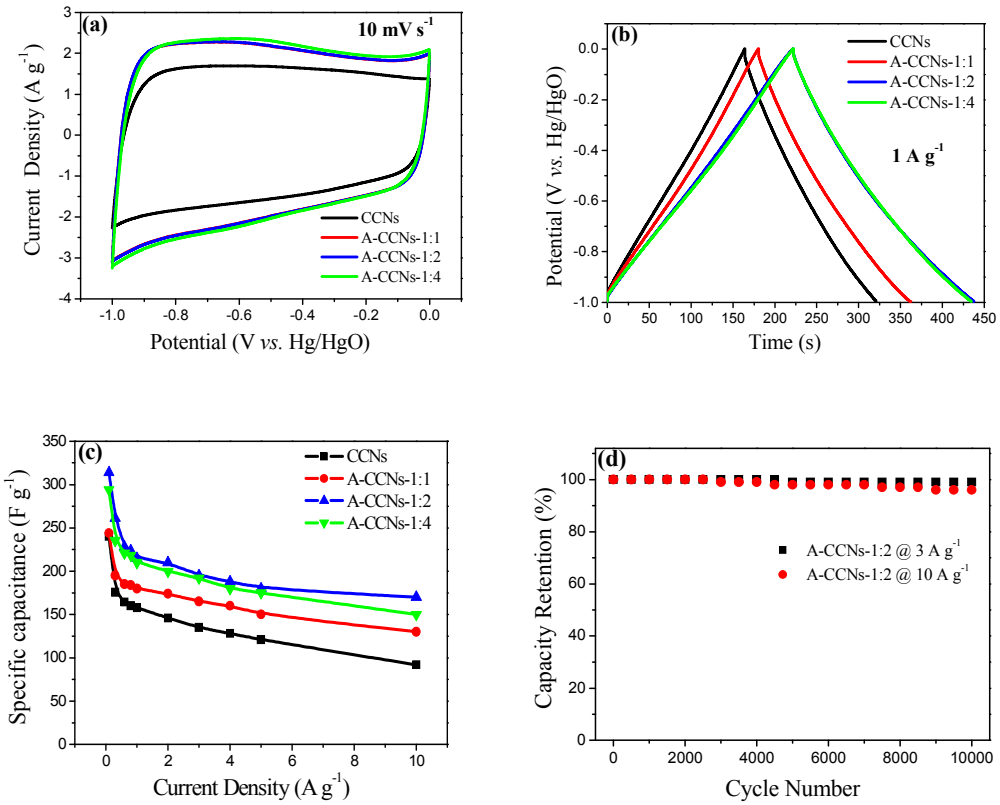

Figure 5

Journal of Materials Chemistry A Accepted Manuscript

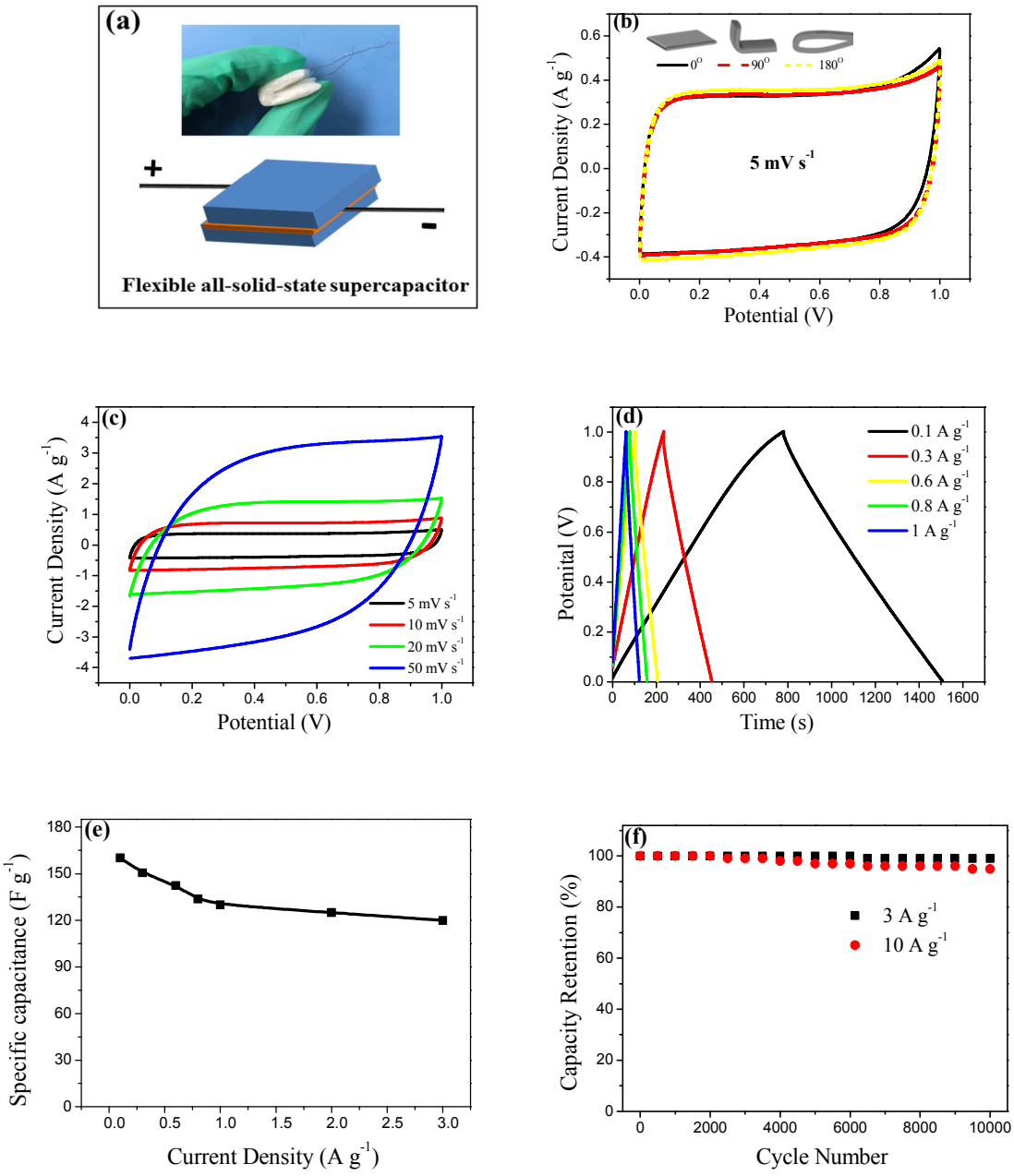

Figure 6

Journal of Materials Chemistry A Accepted Manuscript